HHS Public Access

Author manuscript

Lab Invest. Author manuscript; available in PMC 2009 August 01.

Published in final edited form as:

Lab Invest. 2009 February ; 89(2): 196–208. doi:10.1038/labinvest.2008.124.

Acute kidney injury after hepatic ischemia and reperfusion injury in mice

H. Thomas Lee[1,#], **Sang Won Park**[1], **Mihwa Kim**[1], and **Vivette D. D'Agati**[2]

[1] Department of Anesthesiology, College of Physicians and Surgeons of Columbia University, New York, NY 10032

[2] Department of Pathology, College of Physicians and Surgeons of Columbia University, New York, NY 10032

Abstract

Hepatic ischemia reperfusion (IR) is the leading cause of acute liver failure (ALF) during the perioperative period and patients with ALF frequently develop acute kidney injury (AKI). There is no effective therapy for AKI associated with ALF because pathomechanisms are incompletely characterized, in part due to the lack of an animal model. In this study, we characterize a novel murine model of AKI following hepatic IR. Mice subjected to ~70% liver IR not only developed acute liver dysfunction, but also developed severe AKI 24 hr after liver injury. Mice subjected to liver IR developed histological changes of acute tubular injury including focal proximal tubular cell necrosis involving the S3 segment, cortical tubular ectasia, focal tubular simplification and granular bile/heme cast formation. In addition, there was focal interstitial edema and hyperplasia of the juxtaglomerular apparatus. Inflammatory changes in the kidney after hepatic IR included neutrophil infiltration of the interstitium and upregulation of several pro-inflammatory mRNAs (tumor necrosis factor-α, keratinocyte derived cytokine, monocyte chemotactic protein-1, macrophage inflammatory protein-2, intercellular adhesion molecule-1). In addition, marked renal endothelial cell apoptosis was detected involving peritubular interstitial capillaries, accompanied by increased renal vascular permeability. Finally, there was severe disruption of renal proximal tubule epithelial filamentous-actin. Our results show that AKI rapidly and reproducibly develops in mice after hepatic IR and is characterized by renal tubular necrosis, inflammatory changes and interstitial capillary endothelial apoptosis. Our murine model of AKI after liver injury closely mimics human AKI associated with ALF and may be useful in delineating the mechanisms and potential therapies for this common clinical condition.

Keywords

acute renal failure; apoptosis; endothelium; hepatic ischemia; inflammation; necrosis; neutrophil

[#]Address for Correspondence: H. Thomas Lee, M.D., Ph.D., Associate Professor, Department of Anesthesiology, Anesthesiology Research, Laboratories, Columbia University, P&S Box 46 (PH-5), 630 West 168th Street, New York, NY 10032-3784, Tel: (212) 305-1807 (Lab), Fax: (212) 305-8980, E.Mail: tl128@columbia.edu.

Conflict of interest statement

We declare that no financial conflict of interest exists for each author.

Introduction

Hepatic ischemia reperfusion (IR) injury is a major clinical problem during the perioperative period. Hepatic IR injury is a major cause of acute liver failure (ALF) and is frequently associated with major hepatic resection, liver transplantation, or septic shock (1–3). Acute kidney injury (AKI) occurs frequently in patients with acute liver failure (ALF) and is a serious clinical problem during the perioperative period (4,5). For example, the incidence of AKI in patients with ALF ranges from 40–85% depending on the diagnostic criteria and etiology (4,6). In addition, AKI is a common complication after orthotopic liver transplantation and exponentially increases patient mortality (4). Unfortunately, the pathophysiology of AKI associated with ALF is poorly understood in part due to a lack of diagnostic histological changes or an adequate animal model for this critical clinical syndrome. Moreover, development of AKI after liver injury in mice has never been described in detail.

Previous animal models for AKI associated with liver failure include carbon tetrachloride (CCl_4) injection after bile duct ligation in mice (7) and partial hepatic IR in rats (8). The CCl_4 injection model is limited by the chronic nature of the protocol requiring several (8–12) weeks (whereas human renal failure associated with ALF can develop acutely). The rat model of AKI after liver IR is limited by the modest nature of renal dysfunction after liver IR injury which therefore fails to mimic the severity of human disease (8,9).

In this study, we tested the hypothesis that mice subjected to severe liver IR develop AKI resembling human AKI associated with ALF. We demonstrate that mice subjected to hepatic IR develop AKI in less than 24 hr characterized by proximal tubular necrosis and inflammation. Moreover, renal peritubular endothelial cell apoptosis, peritubular/interstitial neutrophil infiltration, JGA hyperplasia as well as marked disruptions of the kidney tubular actin cytoskeletal architecture were observed. Our results show that mice subjected to liver IR develop AKI rapidly, closely mimicking the time course of this complication in humans.

Methods

Murine model of hepatic IR

After Columbia University IACUC approval, male C57BL/6 mice (25–30g, Harlan, Indianapolis, IN) were anesthetized with intraperitoneal pentobarbital, 50 mg/kg or to effect. Mice were placed under a heating lamp and on a 37°C heating pad. After a midline laparotomy and intraperitoneal application of 20 U heparin, left lateral and median lobes of the liver were subjected to 60 min. of ischemia with a microaneurysm clip occluding the hepatic triad above the bifurcation. This method of partial hepatic ischemia results in a segmental (~70%) hepatic ischemia but spares the right lobe of the liver and prevents mesenteric venous congestion by allowing portal decompression through the right and caudate lobes of the liver (10,11). Preliminary studies showed that 30, 60 or 90 min. of liver ischemia causes mild, moderate or severe liver injury, respectively. The liver was kept moist with gauze soaked in 0.9% normal saline. The body temperature was monitored by an infrared temperature sensor (Linear Laboratories, Fremont, CA) and maintained at 37°C

using a heating lamp and a heating pad. After 60 minutes, the liver was reperfused and the wound closed. Sham operated mice were subjected to laparotomy and identical liver manipulations without the vascular occlusion. Twenty four hr after reperfusion, the liver tissue subjected to IR and both kidneys were collected to measure necrosis, neutrophil infiltration (with immunohistochemistry) and apoptosis (with terminal deoxynucleotidyl transferase-mediated dUTP nick end labeling staining). In some mice, liver and kidneys were collected 4 hr after reperfusion to detect renal inflammation by RT-PCR for pro-inflammatory cytokine mRNAs. We also collected plasma for the measurement of alanine aminotransferase (ALT) and creatinine (Cr) 4 and 24 hr after reperfusion.

Assessment of liver and kidney dysfunction

Plasma ALT was measured by using a Prep-Profile II kit and a VetScan VS2 Point-of-Care Analyzer (Union City, CA) and expressed as Units/Liter (U/L). Renal dysfunction after liver IR injury was assessed by measurement of plasma creatinine by a colorimetric method based on the Jaffe reaction (12).

Histology and quantification of hepatic and renal injury after hepatic IR injury

Twenty four hr after reperfusion, the liver tissue subjected to IR and both kidneys were collected. For histological preparations, explanted murine livers or kidneys were fixed in 10% formalin solution overnight. After automated dehydration through a graded alcohol series, transverse liver slices were embedded in paraffin, sectioned at 4 μm, and stained with hematoxylin-eosin (H&E). To quantify the degree (%) of hepatic necrosis, liver H&E sections were digitally photographed and the percent of necrotic area was quantified with NIH IMAGE (Image-J, 1.37v) software by a person who was unaware of the treatment each sample received. Renal H&E sections were evaluated for renal proximal tubule necrosis and apoptosis, endothelial cell apoptosis, simplification, juxtaglomerular apparatus hypertrophy and cell number by an experienced renal pathologist (VDD) who was blinded to the treatment each animal had received.

Assessment of renal inflammation

Kidney inflammation after hepatic ischemia was determined with detection of neutrophil infiltration by immunohistochemistry 24 hr after hepatic IR as described previously (13–15) and by measuring mRNA encoding markers of inflammation, including keratinocyte derived cytokine (KC), intercellular adhesion molecule-1 (ICAM-1), monocyte chemoattractive protein-1 (MCP-1), macrophage inflammatory protein-2 (MIP-2), and tumor necrosis factor-alpha (TNF-α) 4 hr after liver IR. Both semi-quantitative (13–15) and quantitative real-time RTPCR (Q-RTPCR) were performed. Q-RTPCR was performed with the MyiQ Real Time Detection System (Bio-Rad, Hercules, CA) using SYBR Green I Brilliant Mastermix (Stratagene, La Jolla, CA). The cDNA template was synthesized using Omniscript Reverse Transcriptase and oligo-dT primer (Qiagen, Valencia, CA). Specificity of the amplification was checked by melting curve analysis and by agarose gel electrophoresis. All reactions were performed in duplicate with appropriate negative controls. The Ct values were determined by using M×3000P software. Values were normalized for GAPDH mRNA and relative expression of pro-inflammatory mRNA was calculated with the $\Delta\Delta Ct$ method.

Detection of renal apoptosis with in situ Terminal Deoxynucleotidyl Transferase Biotin-dUTP Nick End-Labeling assay

Twenty four hr after reperfusion, the liver tissue subjected to IR and both kidneys were collected. We used *in situ* terminal deoxynucleotidyl transferase biotin-dUTP nick-end labeling (TUNEL) staining to detect DNA fragmentation in apoptosis as described previously (16,17).

Filamentous (F)-actin staining of liver and kidney sections after liver IR injury

Twenty four hr after reperfusion, the liver tissue subjected to IR and both kidneys were collected. As breakdown of F-actin occurs early after IR, we visualized the F-actin cytoskeleton by staining with phalloidin as an early index of liver as well as renal injury (18,19). We visualized the F-actin cytoskeleton by staining with phalloidin. Twenty four hr after liver IR, liver and kidney tissue were embedded in Tissue-Tek oxytetracycline compound (Fisher Scientific, Pittsburgh, PA) and cut into 5μm sections. To reduce background staining, the sections were incubated in 1% FBS dissolved in PBS for 10 minutes at room temperature. The sections were then stained with Alexafluor 594 (Red)-labeled phalloidin (Invitrogen, Carlsbad, CA) for 30 min at 37°C in a humidified chamber in the dark. Sections were then washed twice in PBS and mounted with Vectashield (Vector Laboratories, Burlingame, CA). F-actin images were visualized with an Olympus IX81 epifluorescence microscope (Tokyo, Japan) and captured and stored using SlideBook 4.2 software (Intelligent Imaging Innovations Inc., Denver, CO) on a personal computer.

Analysis of liver and kidney vascular permeability

Twenty four hr after reperfusion, the liver tissue subjected to IR and both kidneys were collected. Changes in liver and kidney vascular permeability were assessed by quantitating extravasations of Evans blue dye (EBD) into the tissue as described by Awad *et al*. (20) with some modifications. Briefly, 2% EBD (Sigma Biosciences, St. Louis, MO) was administered at a dose of 20 mg/kg iv 24 hr after liver injury. One hour later, mice were killed and perfused through the heart with PBS and EDTA with 10 cc cold saline with heparin (100 U/ml). Liver and kidneys were then removed, allowed to dry overnight at 60°C, and the dry weights were determined. EBD was extracted in formamide (20 ml/g dry tissue; Sigma Biosciences), homogenized, and incubated at 60°C overnight. Homogenized samples were centrifuged at 5,000 *g* for 30 min and the supernatants were measured at 620 and 740 nm in a spectrophotometer. The extravasated EBD concentration was calculated against a standard curve and the data expressed as micrograms of EBD per gram of dry tissue weight.

Protein Determination

Protein contents were determined with a bicinchoninic acid protein assay kit (Pierce Chemical Co., Rockford, IL), using BSA as a standard.

Statistical Analyses

The data were analyzed with Student's *t*-test when comparing means between two groups or with one-way analysis of variance plus Tukey's *post hoc* multiple comparison test to

compare mean values across multiple treatment groups. In all cases, significance was assumed at a probability statistic of <0.05. All data are expressed throughout the text as mean ± S.E.

Reagents

Unless otherwise specified, all reagents were purchased from Sigma (St. Louis, MO).

Results

Acute hepatic and renal dysfunction after liver IR

The survival rate for sham-operated animals and animals subjected to 60 min of liver ischemia and 24 hr reperfusion were 100% (5/5) and 94% (15/16), respectively. Sham-operated C57BL/6 mice had normal plasma ALT and Cr at 4 hr (ALT= 61±12 mg/dL, N=4, and Cr=0.28±0.09 mg/dL, N=4) and 24 hr after surgery (ALT=58±11 U/L, N=5, and Cr=0.31±0.11 mg/dL, N=5). However, C57BL/6 mice subjected to liver IR developed severe liver dysfunction at 4 and 24 hr after hepatic ischemic injury with significantly higher plasma ALT levels (20097±1434 U/L, N=6, $p<0.0001$ and 14560+2275 U/L, N=10, $p<0.0001$, respectively, compared to sham-operated mice). Moreover, C57BL/6 mice subjected to liver IR also developed AKI with significant rises in plasma Cr 4 hr (Cr=0.60±0.09 mg/dL, N=6, $p<0.05$ vs. sham) and 24 hr (Cr=0.91±0.15 mg/dL, N=10, $p<0.05$ vs. sham) after liver IR. Moreover, there was a direct relationship between the severity of liver dysfunction (ALT) and the degree of AKI (Cr) 24 hr after IR ($p<0.0001$ and $r^2=0.8925$, Figure 1). The BUN values also significantly increased in mice subjected to liver ischemia and 24 hr reperfusion (128±10 mg/dL, N=10, $p<0.0001$) compared to the mice subjected to sham surgery (12±2 mg/dL, N=4).

Hepatic IR injury results in histological changes in the kidney

As we observed previously, our model of 60 min. partial hepatic IR injury produced moderate to severe liver necrosis (76±9%, N=10) in all samples examined 24 hr after IR with some sparing of the hepatocytes near the portal traid (Figure 2). We failed to detect liver necrosis in sham-operated animals. When we examined the kidneys from the mice subjected to liver IR, we observed multifocal acute tubular injury including individual cell necrosis involving the juxtamedullary proximal tubules of the S3 segment. In addition the cortical tubules exhibited focal tubular simplification, cytoplasmic vacuolization, dilated lumina and focal granular bile/heme casts, accompanied by mild interstitial edema. Endothelial apoptosis of peritubular capillaries was also visible in H&E sections as linear arrays of apoptotic bodies corresponding to interstitial capillary lining endothelium (Figure 3). Manual counting of cells in the S3 segment of proximal tubules showed significantly higher number of necrotic cells compared to the sham-operated mice (Figure 3). The number of glomeruli with detectable juxtaglomerular apparatus in H&E sections and the number of cells per juxtaglomerular apparatus were both increased after liver IR, indicating hyperplasia of the juxtaglomerular apparatus. (Figure 3 and 4).

Hepatic IR injury increases pro-inflammatory mRNA expression in the liver as well as in the kidney

With RTPCR, we measured the expression of pro-inflammatory cytokine mRNAs in the liver and the kidney 4 hr after liver IR. We showed previously that 60 min. of hepatic ischemia and 4 hr reperfusion resulted in significant upregulation of pro-inflammatory cytokine mRNAs in the liver compared to the sham-operated mice (21) and again demonstrate this finding here (Figure 5A, 5C). We now show that hepatic IR injury was associated with significantly increased pro-inflammatory mRNA expression (ICAM-1, TNF-α, KC, MCP-1 and MIP-2) in the kidney (Figure 5B, 5C) compared to the sham-operated mice.

Hepatic IR injury increases renal neutrophil infiltration 24 hr after IR injury

We showed previously that 60 min. of hepatic ischemia and 24 hr of reperfusion resulted in a significant influx of neutrophils into the liver compared to the sham-operated mice (21). Neutrophil infiltratiopn was not detected in the kidneys from sham-operated mice, however, infiltration was easily visible in the kidneys from mice subjected to liver IR (Figure 6). Neutrophil infiltration was seen in both capillaries and in the interstitial space. Capillary infiltrations were seen in juxtamedullary cortex with extravasations occurring in small foci around peritubular capillaries. Interstitial infiltrations were more prominent involving the subcapsular and outer cortical regions.

Hepatic IR injury increases renal apoptosis 24 hr after IR injury

When the kidneys isolated from mice subjected to liver IR were examined for apoptosis, we observed significantly increased number of apoptotic nuclei (TUNEL positive cells, Figure 7). TUNEL positive cells were heavily localized to the perivascular area rather than to the renal proximal tubule cells (cells typically showing apoptotic changes after renal IR). In order to clarify the location of TUNEL positive cells, we double-stained the kidney sections with hematoxylin and TUNEL stain. Figure 8 shows again that the TUNEL positive cells are localized mostly in the perivascular area. We further confirmed that the TUNEL positive cells are endothelial cells by staining parallel kidney sections with TUNEL and CD34 (an endothelial cell marker, Abcam Inc., Cambridge, MA) and confirmed that TUNEL positive cells also stained for CD34 (Figure 9, representative of 4 representative serial sections).

Hepatic IR disrupts both hepatocyte and renal tubule F-actin architecture

Liver F-actin staining in sham-operated mice shows localization to the hepatocyte periphery and around the bile canaliculus. As expected, 60 min. of liver ischemia and 24 hr of reperfusion resulted in severe disruption of liver parenchymal F-actin compared to the sham-operated mice (Figure 10, representative of 6 experiments). Surprisingly, liver IR injury also resulted in a severe loss of F-actin in renal proximal tubules. In Figure 10, 24 hr post-hepatic IR induced disruptions of the F-actin cytoskeleton in renal proximal tubular epithelial cells are shown. C57BL/6 Mice were subjected to sham surgery showed intense stain in the tubular epithelial and in the basal plasma membrane. In contrast, kidneys from mice subjected to liver IR showed loss of F-actin staining in the tubular epithelial cells.

Hepatic IR increases vascular permeability in the liver as well as in the kidneys

We measured liver and kidney vascular permeability after liver IR with EBD injection. EBD binds to plasma proteins and its appearance in extravascular tissues reflects an increase in vascular permeability. Analysis of EBD extravasations in sham-operated mice and mice subjected to liver IR is shown in Figure 11. Liver IR not only increased the EBD content in the liver (337±43 μg EBD/g dry kidney, N=10) compared to sham-operated mice (45±8 μg EBD/g dry kidney, N=6, $p<0.001$) but also increased the EBD content in the kidney as well (liver IR EBD: 77±6 μg EBD/g dry kidney, N=10 vs, sham EBD: 46±9 μg EBD/g dry kidney, N=6, $p<0.02$).

Discussion

The major new finding of this study is that mice subjected to a clinically relevant model of liver IR injury developed severe AKI. Liver IR induced AKI in mice shared similar histological changes observed in human AKI associated with liver failure including JGA hyperplasia, renal tubule necrosis, proximal tubule simplification and vacuolization. In addition, we showed that mice with AKI displayed marked renal endothelial apoptosis and F-actin disruption in the kidney. Moreover, liver IR also caused renal cortical pro-inflammatory mRNA expression and infiltration of PMNs.

Hepatic IR induced ALF is a very common clinical problem and frequently leads to dysfunction of remote organs including the lung, heart and kidney (6,22–24). AKI associated with liver failure is a grave clinical problem with high mortality rate. In fact, the diagnosis of AKI in patients with liver failure implies a significant increase in mortality and morbidity (4,25–27). Supportive therapies for AKI associated with liver failure are limited to hydration, blood pressure support and short-term hemodialysis until renal function recovers. In fact, for hepatorenal syndrome (a type of AKI associated with ALF), liver transplantation is the only definitive treatment (6). Unfortunately, the pathogenesis of AKI associated with liver failure is poorly understood, largely due to a lack of a reproducible and reliable animal model. A reproducible animal model would allow preclinical testing of therapeutic approaches that could lead to human therapy. In this study, we describe a model of AKI in mice induced with liver IR that is reproducible, rapid to develop (in less than 24 hr) and mimics the histological (renal tubular damage, apoptosis, necrosis and JGA hyperplasia) as well as biochemical (plasma creatinine, inflammatory markers) changes observed with human AKI associated with ALF (6).

Although the pathophysiological and biochemical mechanisms of AKI associated with liver failure are not fully understood, the initiating event appears to be portal hypertension–induced splanchnic vasodilatation with subsequent intrarenal vasoconstriction (6,25,26). Patients with acute liver failure develop hypotension secondary to splanchnic and peripheral vasodilation and hypovolemia (6). The renin-angiotensin system is activated due to a reduced systemic blood pressure and splanchnic vasodilation (6,7). Upregulation of renin-angiotensin system leads to severe reduction glomerular filtration rate, urinary sodium excretion and free water excretion. It has been proposed that intense intra-renal ischemia subsequent to renin-angiotensin activation leads to renal tubular necrosis and renal dysfunction. In this study, we show significant hyperplasia of juxtaglomerular apparatus

with increased cellularity in mice subjected to liver IR. These changes are similar to the changes seen in human AKI associated with ALF reflecting intense upregulation of the renin-angiotensin system (6,25). We also show several hallmark signs of renal damage due to intense intrarenal vasoconstriction including renal tubular necrosis, tubular simplification and vacuolization.

However, other mechanisms may play important roles in the pathogenesis of renal dysfunction with ALF. Systemic inflammatory response after liver IR may induce renal injury (6,22). After liver IR injury, circulating pro-inflammatory cytokines and transcription factors including TNF-α and HMGB1 increase significantly (23,28,29). Release of pro-inflammatory cytokines such as TNF-α and HMGB1 from the liver may promote inflammatory changes in the kidney after liver IR (22,28,29). These pro-inflammatory factors can upregulate endothelial adhesion molecules in distant organs including the kidney. Upregulation of renal endothelial adhesion molecules including E-selectin, P-selectin, and ICAM-1 promotes leukocyte recruitment and extravasations to the renal interstitial space (30,31). In addition, circulating bile acids, endotoxin and circulating immune complexes may contribute to the development of AKI (6). Combined, these contributing factors may potentiate systemic inflammation leading to renal injury and renal PMN infiltration.

The endothelial barrier serves to protect against AKI by regulating leukocyte recruitment to the areas of injury (1,30). In this study, we were surprised to observe a marked endothelial cell apoptosis in the kidney after liver IR (Figs. 7 and 8). Apoptosis is an important contributor in the development of renal failure (32,33). Apoptotic cell death represents the execution of an ATP-dependent death program often initiated by death ligand/death receptor interactions, such as Fas ligand with Fas, which leads to a caspase activation and cleavage of nuclear materials such as DNA and PARP (34,35). After liver IR, we show that endothelial cell apoptosis in the kidney was much more prominent than the proximal tubule cell apoptosis. This is in contrast to the findings after renal IR where proximal tubule cell apoptosis predominates. Endothelial cell death due to apoptosis would impair defense against leukocyte invasion into the kidney leading to a further exacerbation of renal injury. The results of our study suggest that reducing endothelial cell death may limit renal injury associated with ALF.

In this study, we demonstrate not only significant endothelial cell apoptosis but also recruitment of PMNs to the kidney after liver IR. Neutrophils are activated during and after liver ischemia and activated neutrophils attach to and then transverse the renal capillary endothelium into the subendothelial space, where they release enzymes and cytokines, causing direct renal injury and the recruitment of other injurious cells, such as monocytes and macrophages (36,37). Weakened endothelial defenses after liver IR may potentiate the PMN infiltration and conversely, increasing the survival of endothelial cells after liver IR may limit PMN infiltration into the kidney and improve renal function. Future studies with endothelial stabilizing agents (such as activated protein C or sphingosine-1-phosphate) will determine whether protecting endothelial integrity will reduce renal injury after liver IR injury.

Ischemia reperfusion injury *in vivo* results in degradation of F-actin. Breakdown of F-actin contributes to the pathophysiology of organ dysfunction after ischemia reperfusion injury or sepsis (38). Whereas we were not surprised to see changes in liver F-actin content after liver IR (Fig. 9), we were surprised to demonstrate that renal F-actin breakdown occurs with liver IR. Actin cytoskeletal damage contributes significantly to the development of AKI (38,39). Moreover, F-actin disruption promotes apoptosis in several cell lines (40). Therefore, loss of actin cytoskeleton may have contributed to the development of renal tubular and endothelial apoptosis after liver IR.

We demonstrate in this study that plasma ALT and Cr has a direct and linear relationship: mice with higher ALT showed increased renal dysfunction after liver IR. However, we also noted that the degree of renal dysfunction was mild when the plasma ALT levels were below 10000 U/L. Behrends et al. (8) recently studied the renal dysfunction after extensive liver IR injury in rats. In their study, rats subjected to 75 min. of partial liver IR developed acute liver dysfunction at 24 hr. However, the degree of renal dysfunction in their rat model was mild with modest increases in plasma creatinine. They also noted upregulation of ICAM-1 mRNA expression over control animals but no changes in renal MCP-1, MIP2 and iNOS expression were noted. Correspondingly, the kidneys from rats subjected to liver IR showed little morphological damage and they failed to see increases in apoptosis (caspase-3) and neutrophil infiltration (myeloperoxidase activity). Their study confirms previous observations in rats that renal dysfunction was mild with little or no histological changes after liver IR (9,41). Polat *et al*. also reported that 45 min. of liver ischemia resulted in mild renal dysfunction without detectable changes in renal morphology (9). The reason for this discrepancy between our mouse model and the previous rat model is unclear. However, in the study by Behrends et al. (8), plasma ALT rose only to ~6800 U/L whereas in our mouse model, the plasma ALT rose much higher (~15–20000 U/L). Longer liver ischemic period (e.g., 90 min.) in a rat is usually lethal (unpublished observations). Therefore, it appears that the murine model is better suited as model of liver failure induced AKI than the rat model.

Some investigators utilized carbon tetrachloride (CCl_4) induced cirrhosis as a model of liver failure induced renal injury (7). Our model has several advantages over this model as our model is more clinically relevant, does not require administration of a tubular toxin, and results in rapid and severe AKI. The CCl_4 injection model is limited by the chronic nature of the protocol requiring several weeks (whereas human AKI can develop in less than a week). Moreover, full blown renal dysfunction does not usually occur until day #3 with the CCl_4 model whereas we can produce liver failure induced AKI in less than 24 hr.

To our knowledge, this is the first study utilizing mice to develop a model of AKI after acute liver dysfunction. Our model of AKI after liver IR closely mimics human AKI associated with ALF in terms of severity and the acute nature of renal dysfunction as well as similarities in histological changes. Utilization of mice has further advantages in that genetically modified mice are available to complement pharmacological approaches in studying the signaling mechanisms as well as examining potential therapies for AKI associated with ALF.

Serum creatinine is the most commonly used clinical indicator of glomerular filtration rate but its reliability as a measurement of glomerular filtration rate may be limited by several factors after acute liver injury. One of the main functional consequences of acute liver injury is a dramatic reduction in serum protein level which influences the intravascular volume and glomerular filtration rate. Acute liver injury actually can lead to low serum creatinine due to decreased hepatic conversion of creatine to creatinine, decreased dietary protein intake and increased renal tubular secretion of creatinine. The increased fraction of creatinine excretion by tubular secretion in the setting low GFR also diminishes the reliability of creatinine as a marker of renal dysfunction. Consequently, the plasma creatinine values reported in this study in mice (0.91±0.15 mg/dL) may actually underestimate the degree of acute kidney injury associated with liver IR. Our measurements of plasma BUN correlated less well with renal function, probably because of interference with the urea cycle and hepatic metabolism after liver IR.

In summary, we have developed a novel murine model of AKI after liver IR, which closely approximates the human disease, characterized by renal tubular necrosis, endothelial cell apoptosis, PMN infiltration and JGA hyperplasia. Our model should provide a useful experimental context to delineate the mechanisms of AKI after liver IR and evaluate potential pharmacological therapies. Our study is the first to characterize the histological changes in detail and to demonstrate marked endothelial apoptosis and F-actin destruction in AKI associated with acute liver injury. It remains to be determined in future studies whether stabilization of endothelial cells would protect against AKI after liver IR injury.

Acknowledgments

This work was supported by National Institute of Health Grant RO1 DK-58547

References

1. Teoh NC, Farrell GC. Hepatic ischemia reperfusion injury: pathogenic mechanisms and basis for hepatoprotection. J Gastroenterol Hepatol. 2003; 18:891–902. [PubMed: 12859717]
2. Serracino-Inglott F, Habib NA, Mathie RT. Hepatic ischemia-reperfusion injury. Am J Surg. 2001; 181:160–166. [PubMed: 11425059]
3. Fondevila C, Busuttil RW, Kupiec-Weglinski JW. Hepatic ischemia/reperfusion injury--a fresh look. Exp Mol Pathol. 2003; 74:86–93. [PubMed: 12710939]
4. Betrosian AP, Agarwal B, Douzinas EE. Acute renal dysfunction in liver diseases. World J Gastroenterol. 2007; 13:5552–5559. [PubMed: 17948928]
5. Arroyo V, Fernandez J, Gines P. Pathogenesis and treatment of hepatorenal syndrome. Semin Liver Dis. 2008; 28:81–95. [PubMed: 18293279]
6. Davis CL, Gonwa TA, Wilkinson AH. Pathophysiology of renal disease associated with liver disorders: implications for liver transplantation. Part I. Liver Transpl. 2002; 8:91–109. [PubMed: 11862584]
7. Rivera-Huizar S, Rincon-Sanchez AR, Covarrubias-Pinedo A, Islas-Carbajal MC, Gabriel-Ortiz G, Pedraza-Chaverri J, Alvarez-Rodriguez A, Meza-Garcia E, Armendariz-Borunda J. Renal dysfunction as a consequence of acute liver damage by bile duct ligation in cirrhotic rats. Exp Toxicol Pathol. 2006; 58:185–195. [PubMed: 16829063]
8. Behrends M, Hirose R, Park YH, Tan V, Dang K, Xu F, Park SH, Niemann CU. Remote renal injury following partial hepatic ischemia/reperfusion injury in rats. J Gastrointest Surg. 2008; 12:490–495. [PubMed: 17701074]

9. Polat C, Tokyol C, Kahraman A, Sabuncuoglu B, Yilmaz S. The effects of desferrioxamine and quercetin on hepatic ischemia-reperfusion induced renal disturbance. Prostaglandins Leukot Essent Fatty Acids. 2006; 74:379–383. [PubMed: 16698257]
10. Lappas CM, Day YJ, Marshall MA, Engelhard VH, Linden J. Adenosine A2A receptor activation reduces hepatic ischemia reperfusion injury by inhibiting CD1d-dependent NKT cell activation. J Exp Med. 2006; 203:2639–2648. [PubMed: 17088433]
11. Day YJ, Marshall MA, Huang L, McDuffie MJ, Okusa MD, Linden J. Protection from ischemic liver injury by activation of A2A adenosine receptors during reperfusion: inhibition of chemokine induction. Am J Physiol Gastrointest Liver Physiol. 2004; 286:G285–G293. [PubMed: 14715520]
12. SLOT C. Plasma creatinine determination. A new and specific Jaffe reaction method. Scand J Clin Lab Invest. 1965; 17:381–387. [PubMed: 5838275]
13. Joo JD, Kim M, Horst P, Kim J, D'Agati VD, Emala CW Sr, Lee HT. Acute and delayed renal protection against renal ischemia and reperfusion injury with A1 adenosine receptors. Am J Physiol Renal Physiol. 2007; 293:F1847–F1857. [PubMed: 17928414]
14. Kim M, Kim M, Kim N, D'Agati VD, Emala CW Sr, Lee HT. Isoflurane mediates protection from renal ischemia-reperfusion injury via sphingosine kinase and sphingosine-1-phosphate-dependent pathways. Am J Physiol Renal Physiol. 2007; 293:F1827–F1835. [PubMed: 17898040]
15. Lee HT, Gallos G, Nasr SH, Emala CW. A1 adenosine receptor activation inhibits inflammation, necrosis, and apoptosis after renal ischemia-reperfusion injury in mice. J Am Soc Nephrol. 2004; 15:102–111. [PubMed: 14694162]
16. Gallos G, Ruyle TD, Emala CW, Lee HT. A1 adenosine receptor knockout mice exhibit increased mortality, renal dysfunction, and hepatic injury in murine septic peritonitis. Am J Physiol Renal Physiol. 2005; 289:F369–F376. [PubMed: 15784841]
17. Gallos G, Jones dr, Nasr SH, Emala CW, Lee HT. Local anesthetics reduce mortality and protect against renal and hepatic dysfunction in murine septic peritonitis. Anesthesiology. 2004; 101:902–911. [PubMed: 15448523]
18. Molitoris BA. Putting the actin cytoskeleton into perspective: pathophysiology of ischemic alterations. Am J Physiol. 1997; 272:F430–F433. [PubMed: 9140042]
19. Molitoris BA. Ischemia-induced loss of epithelial polarity: potential role of the actin cytoskeleton. Am J Physiol. 1991; 260:F769–F778. [PubMed: 2058700]
20. Awad AS, Ye H, Huang L, Li L, Foss FW Jr, Macdonald TL, Lynch KR, Okusa MD. Selective sphingosine 1-phosphate 1 receptor activation reduces ischemia-reperfusion injury in mouse kidney. Am J Physiol Renal Physiol. 2006; 290:F1516–F1524. [PubMed: 16403835]
21. Kim J, Kim M, Song JH, Lee HT. Endogenous A1 adenosine receptors protect against hepatic ischemia reperfusion injury in mice. Liver Transpl. 2008; 14:845–854. [PubMed: 18324658]
22. Tanaka Y, Maher JM, Chen C, Klaassen CD. Hepatic ischemia-reperfusion induces renal heme oxygenase-1 via NF-E2-related factor 2 in rats and mice. Mol Pharmacol. 2007; 71:817–825. [PubMed: 17151289]
23. Wanner GA, Ertel W, Muller P, Hofer Y, Leiderer R, Menger MD, Messmer K. Liver ischemia and reperfusion induces a systemic inflammatory response through Kupffer cell activation. Shock. 1996; 5:34–40. [PubMed: 8821101]
24. Weinbroum AA, Hochhauser E, Rudick V, Kluger Y, Sorkine P, Karchevsky E, Graf E, Boher P, Flaishon R, Fjodorov D, Niv D, Vidne BA. Direct induction of acute lung and myocardial dysfunction by liver ischemia and reperfusion. J Trauma. 1997; 43:627–633. [PubMed: 9356059]
25. Wadei HM, Mai ML, Ahsan N, Gonwa TA. Hepatorenal syndrome: pathophysiology and management. Clin J Am Soc Nephrol. 2006; 1:1066–1079. [PubMed: 17699328]
26. Schepke M. Hepatorenal syndrome: current diagnostic and therapeutic concepts. Nephrol Dial Transplant. 2007; 22(Suppl 8):viii2–viii4. [PubMed: 17890258]
27. Genzini T, Torricelli FC. Hepatorenal syndrome: an update. Sao Paulo Med J. 2007; 125:50–56. [PubMed: 17505686]
28. Tsung A, Hoffman RA, Izuishi K, Critchlow ND, Nakao A, Chan MH, Lotze MT, Geller DA, Billiar TR. Hepatic ischemia/reperfusion injury involves functional TLR4 signaling in nonparenchymal cells. J Immunol. 2005; 175:7661–7668. [PubMed: 16301676]

29. Levy RM, Mollen KP, Prince JM, Kaczorowski DJ, Vallabhaneni R, Liu S, Tracey KJ, Lotze MT, Hackam DJ, Fink MP, Vodovotz Y, Billiar TR. Systemic inflammation and remote organ injury following trauma require HMGB1. Am J Physiol Regul Integr Comp Physiol. 2007; 293:R1538–R1544. [PubMed: 17652366]

30. Sutton TA, Mang HE, Campos SB, Sandoval RM, Yoder MC, Molitoris BA. Injury of the renal microvascular endothelium alters barrier function after ischemia. Am J Physiol Renal Physiol. 2003; 285:F191–F198. [PubMed: 12684225]

31. Molitoris BA, Sandoval R, Sutton TA. Endothelial injury and dysfunction in ischemic acute renal failure. Crit Care Med. 2002; 30:S235–S240. [PubMed: 12004242]

32. Lieberthal W, Koh JS, Levine JS. Necrosis and apoptosis in acute renal failure. Semin Nephrol. 1998; 18:505–518. [PubMed: 9754603]

33. Daemen MA, de Vries B, Buurman WA. Apoptosis and inflammation in renal reperfusion injury. Transplantation. 2002; 73:1693–1700. [PubMed: 12084988]

34. Ueda N, Kaushal GP, Shah SV. Apoptotic mechanisms in acute renal failure. Am J Med. 2000; 108:403–415. [PubMed: 10759097]

35. Lee HT, Kim M, Jan M, Penn RB, Emala CW. Renal tubule necrosis and apoptosis modulation by A1 adenosine receptor expression. Kidney Int. 2007

36. Okusa MD. The inflammatory cascade in acute ischemic renal failure. Nephron. 2002; 90:133–138. [PubMed: 11818695]

37. Klausner JM, Paterson IS, Goldman G, Kobzik L, Rodzen C, Lawrence R, Valeri CR, Shepro D, Hechtman HB. Postischemic renal injury is mediated by neutrophils and leukotrienes. Am J Physiol. 1989; 256:F794–F802. [PubMed: 2541628]

38. Molitoris BA. Actin cytoskeleton in ischemic acute renal failure. Kidney Int. 2004; 66:871–883. [PubMed: 15253754]

39. Kellerman PS, Norenberg SL, Jones GM. Early recovery of the actin cytoskeleton during renal ischemic injury in vivo. Am J Kidney Dis. 1996; 27:709–714. [PubMed: 8629632]

40. White SR, Williams P, Wojcik KR, Sun S, Hiemstra PS, Rabe KF, Dorscheid DR. Initiation of apoptosis by actin cytoskeletal derangement in human airway epithelial cells. Am J Respir Cell Mol Biol. 2001; 24:282–294. [PubMed: 11245627]

41. Kudo Y, Egashira T, Takayama F, Yamanaka Y, Shimada T. Investigation of the renal injury caused by liver ischemia-reperfusion in rats. Arch Toxicol. 1993; 67:502–509. [PubMed: 8240000]

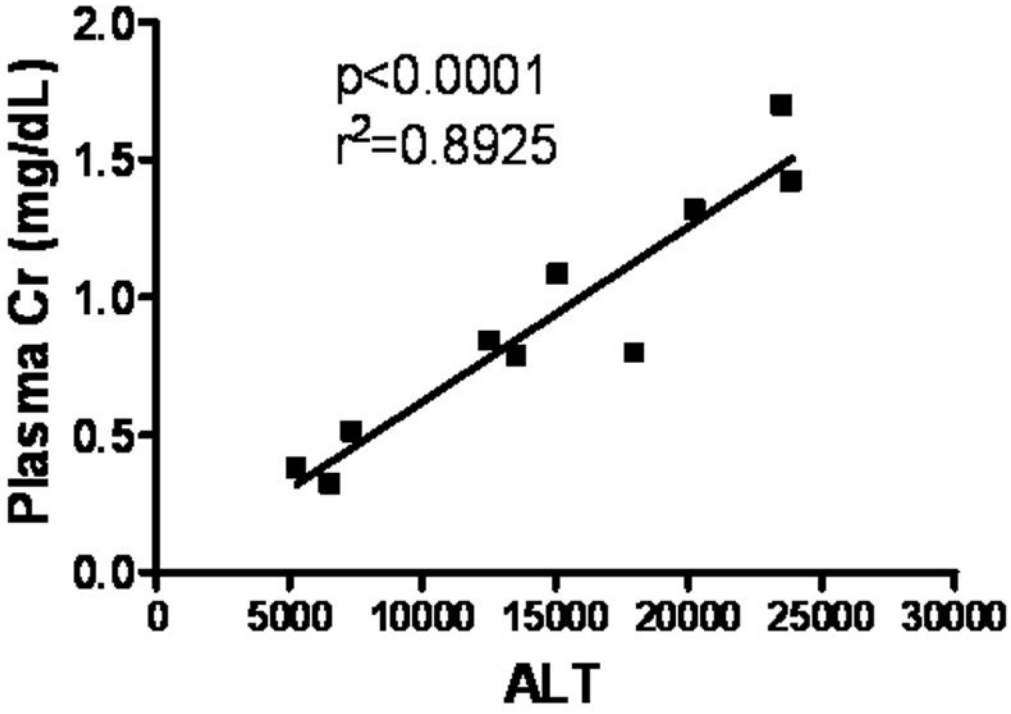

Figure 1.

Correlation between plasma ALT and creatinine (Cr) values ($p<0.0001$ and $r^2= 0.8925$). C57BL/6 mice were subjected to 60 min. liver ischemia and 24 hr reperfusion, and plasma collected for ALT and creatinine assays (N=10).

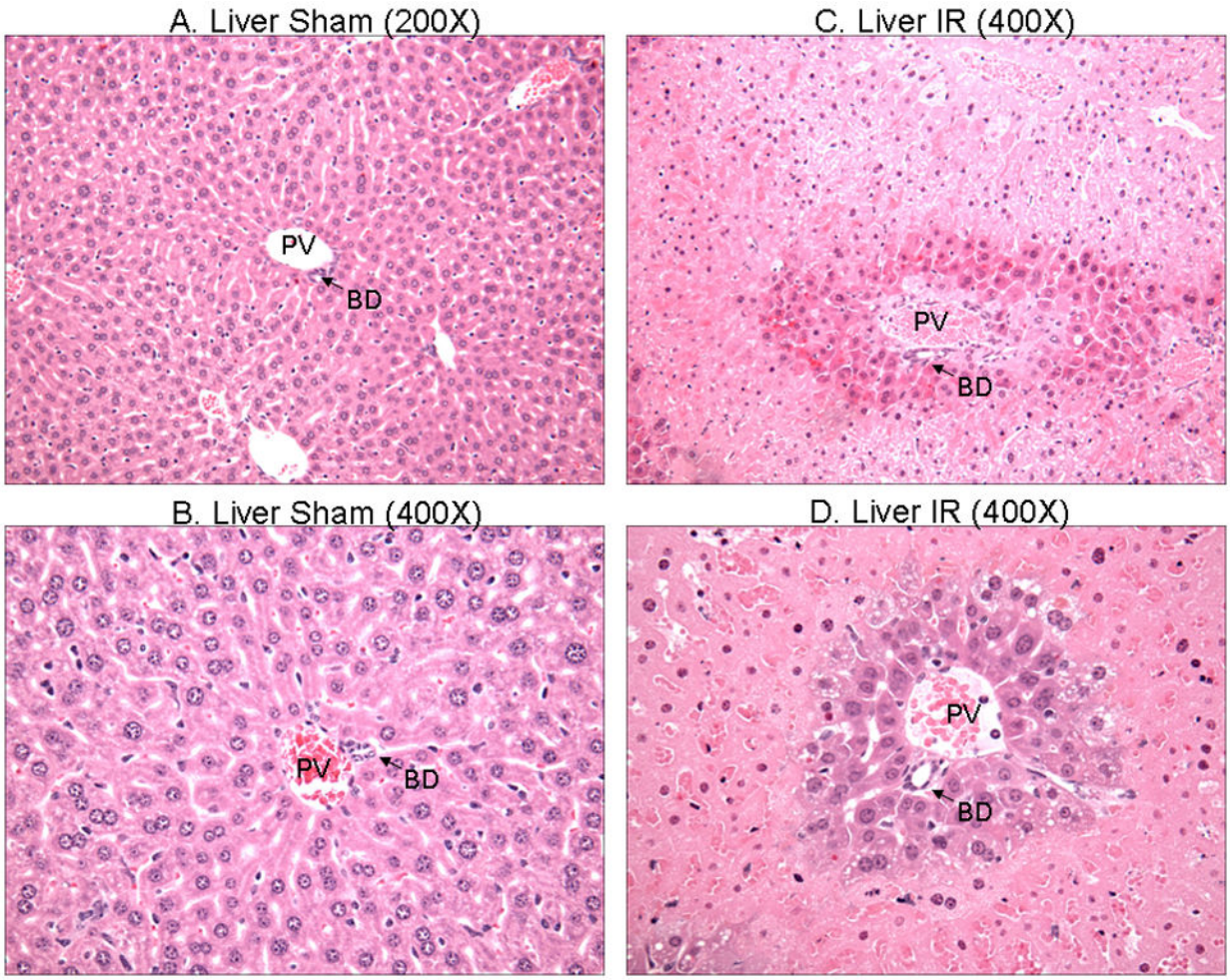

Figure 2.

Representative photomicrographs of 5 experiments (hematoxylin and eosin staining, magnification 200X (A and C) and 400X (B and D) of mice subjected to sham-operation or to liver IR injury. Sham operated animals show normal-appearing hepatocyte parenchyma (A and B). Following liver IR, there is severe hepatocyte necrosis and loss of normal liver architecture with some sparing of the hepatocytes near the portal triad. PV=portal vein. BD=bile duct.

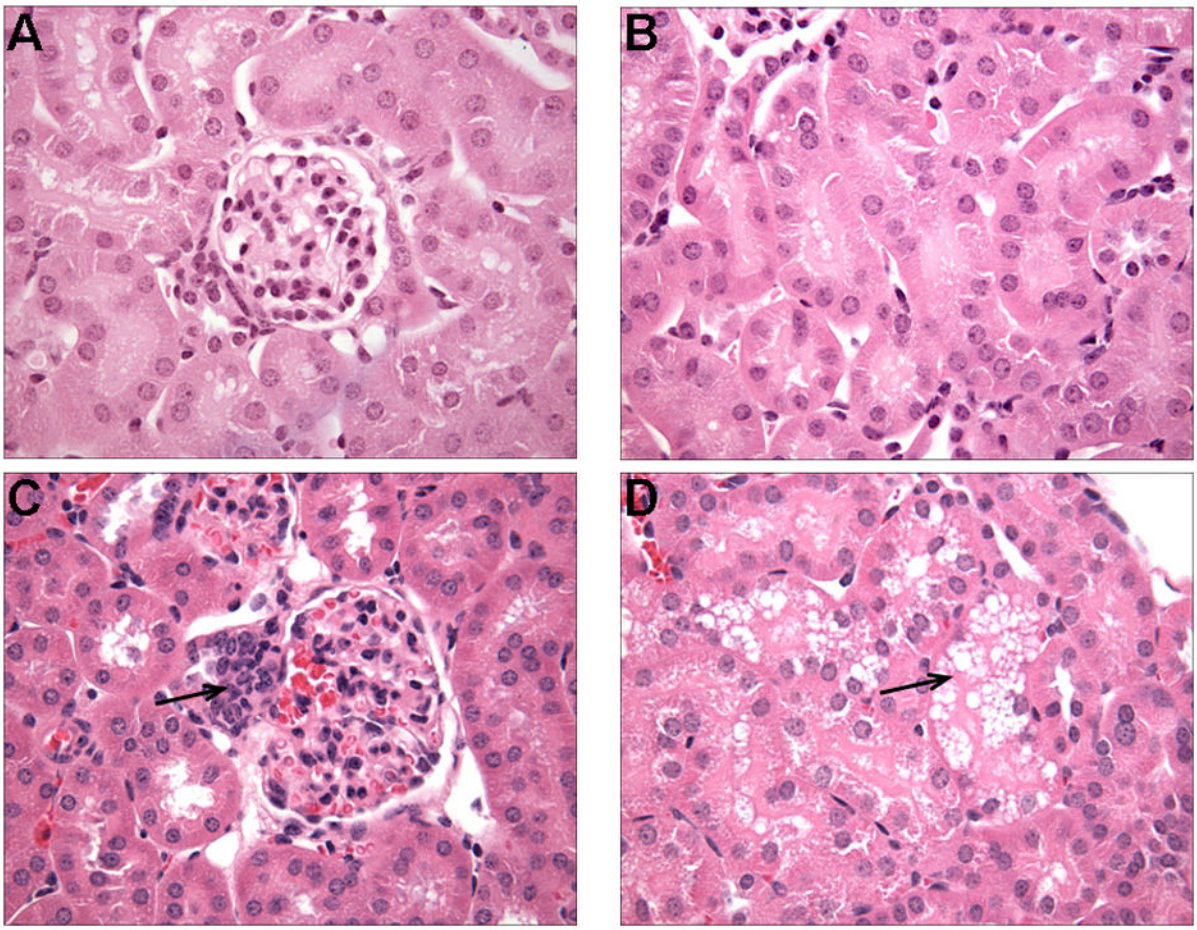

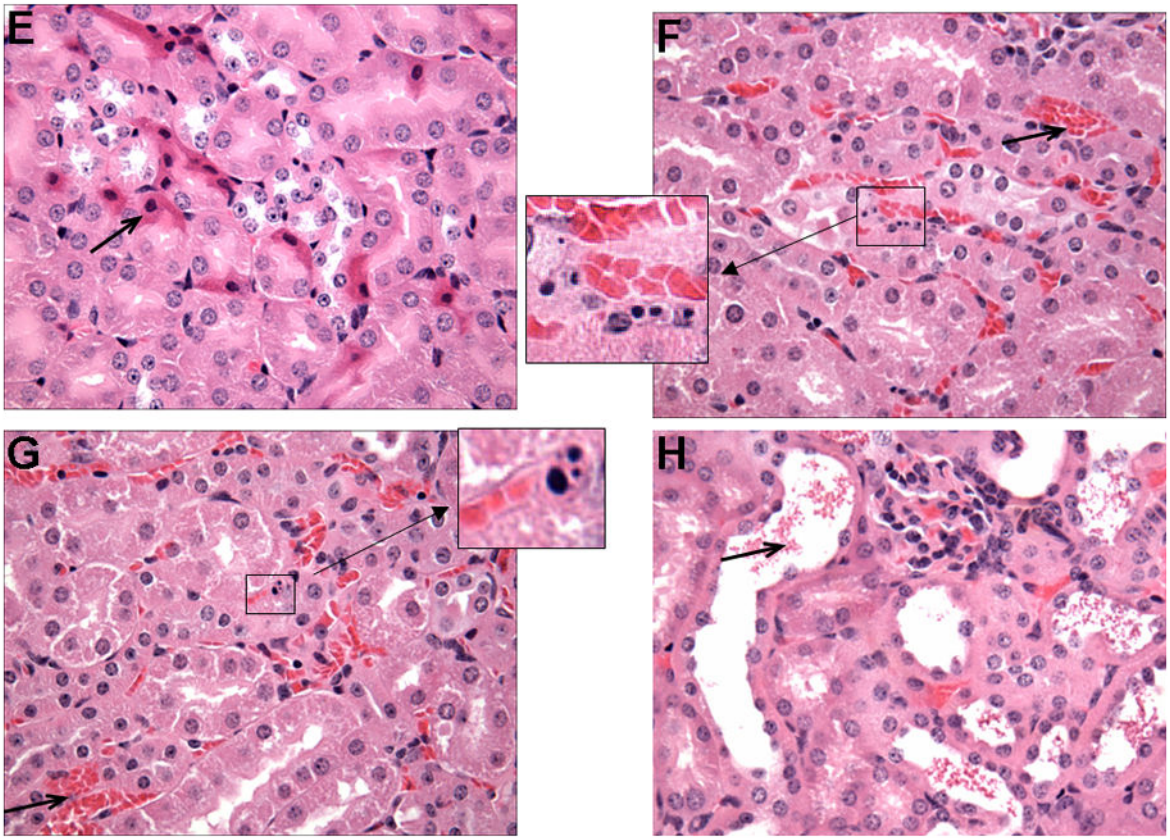

Figure 3.

Representative photomicrographs of 6 experiments (hematoxylin and eosin staining, magnification 600X) of mice subjected to sham-operation or to liver IR injury. Sham operated animals show normal-appearing glomeruli (A) and tubules (B). Following liver IR, many glomeruli display prominent hyperplasia of the juxtaglomerular apparatus (arrow) located at the glomerular hilus (C). There is focal coarse clear cytoplasmic vacuolization (arrow) of proximal tubular epithelial cells (D). Some cortical tubular cells display acute epithelial injury with cellular condensation and cytoplasmic hypereosinophilia (long arrow) and shrunken, hyperchromatic nuclei (insert expanded) (E). There is focal apoptosis of interstitial capillary endotheial cells (insert expanded) with marked vascular stasis within the interstitial capillary lumina (long arrow) (F, G). We also observed focal tubular dilatation with intraluminal shedding of cytoplasmic debris and formation of granular eosinophilic casts (arrow) (H).

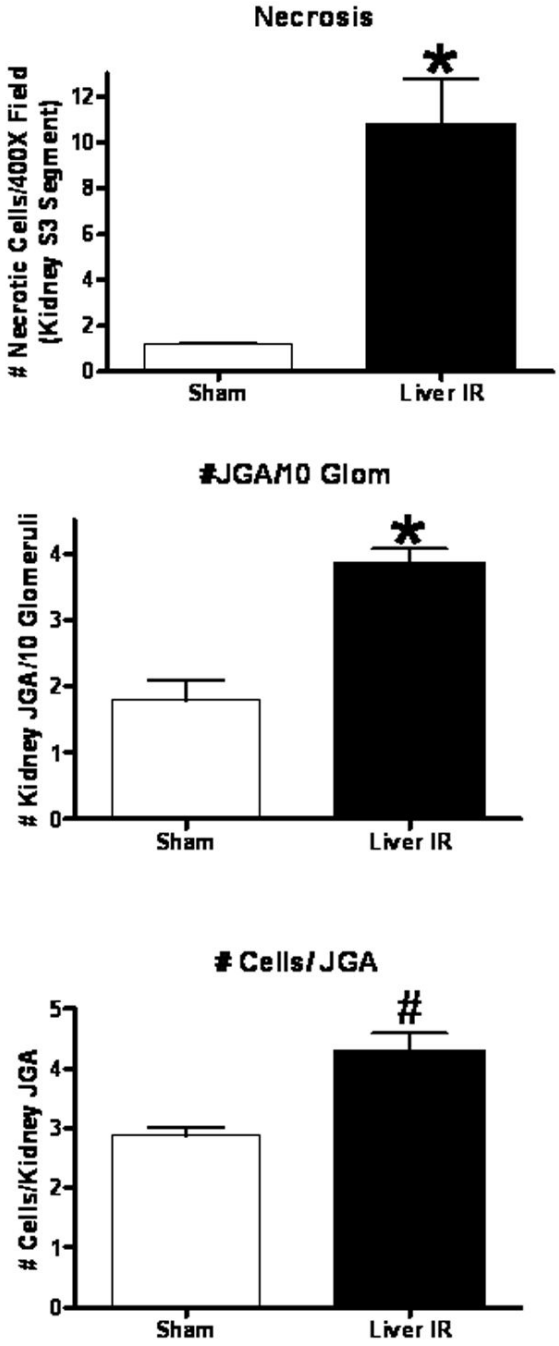

Figure 4.

Renal histological assessment after liver IR in C57BL/6 mice. Mice were subjected to sham-operation (N=5) or to liver IR (N=8). Twenty-four hr later, mice subjected to liver IR showed increased number of necrotic S3 proximal tubules per 400X field (A), increased number of juxtaglomerular apparatus (JGA) per 10 glomeruli counted (B) and increased number of cells per JGA. * $p<0.01$ vs. sham-operated mice. #$p<0.05$ vs. sham-operated mice. Data presented as mean ± SEM.

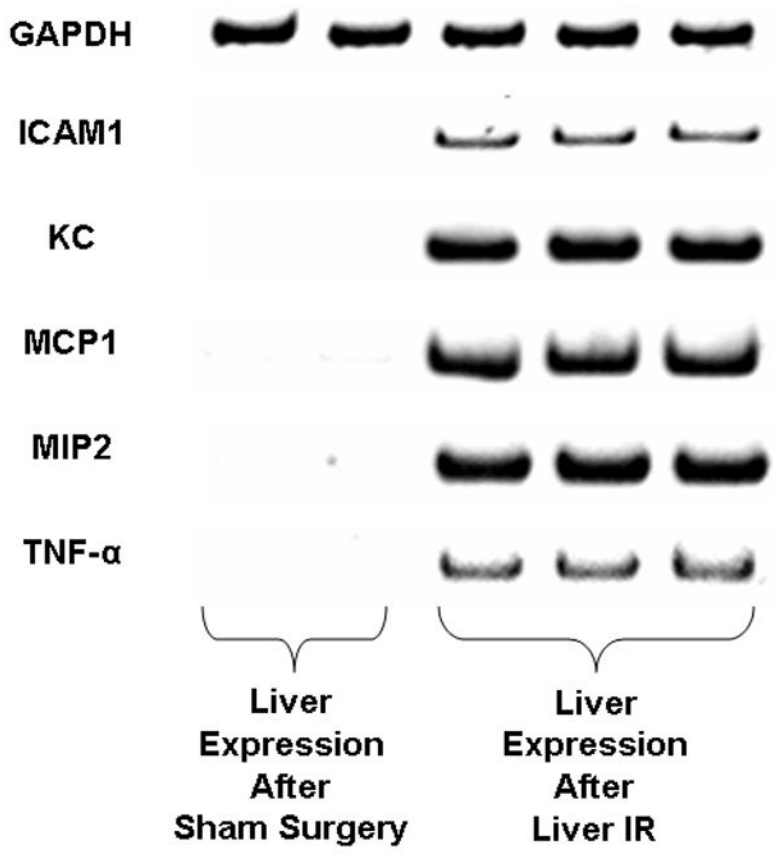

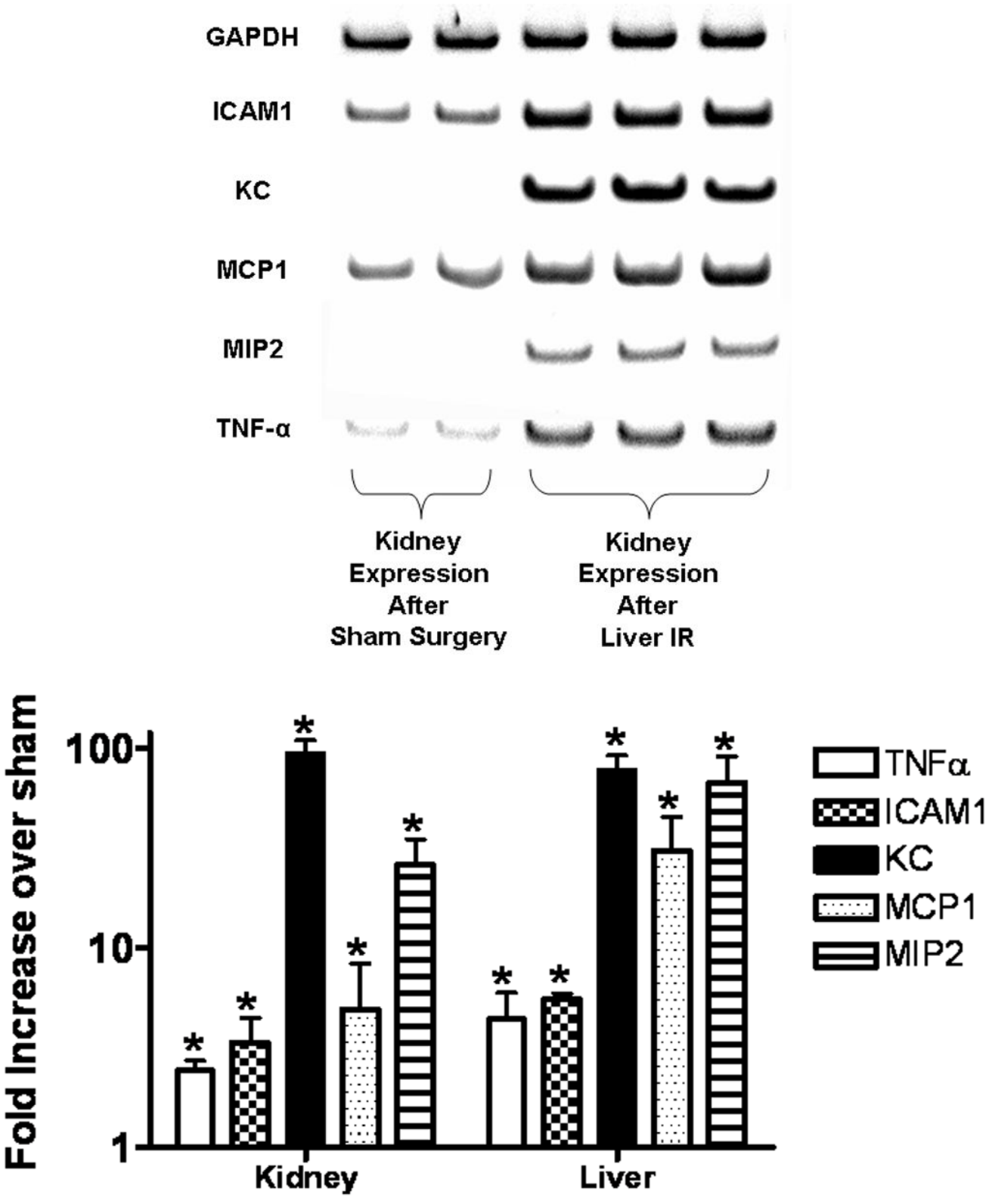

Figure 5.

Representative gel images of semi-quantitative RT-PCR of the pro-inflammatory markers ICAM-1, KC, MCP-1, MIP-2 and TNF-α from liver tissues (A) or from renal cortices (B) of C57BL/6 mice subjected to sham-operation or to liver IR (60 min. ischemia and 4 hr reperfusion). Fold increases in pro-inflammatory mRNAs (in log10 scale) normalized to GAPDH from QRTPCR reactions for each indicated mRNA (N=4 for sham and N=4 for liver IR) are shown (C). * $p<0.05$ vs. sham-operated mice. Error bars represent 1 SEM.

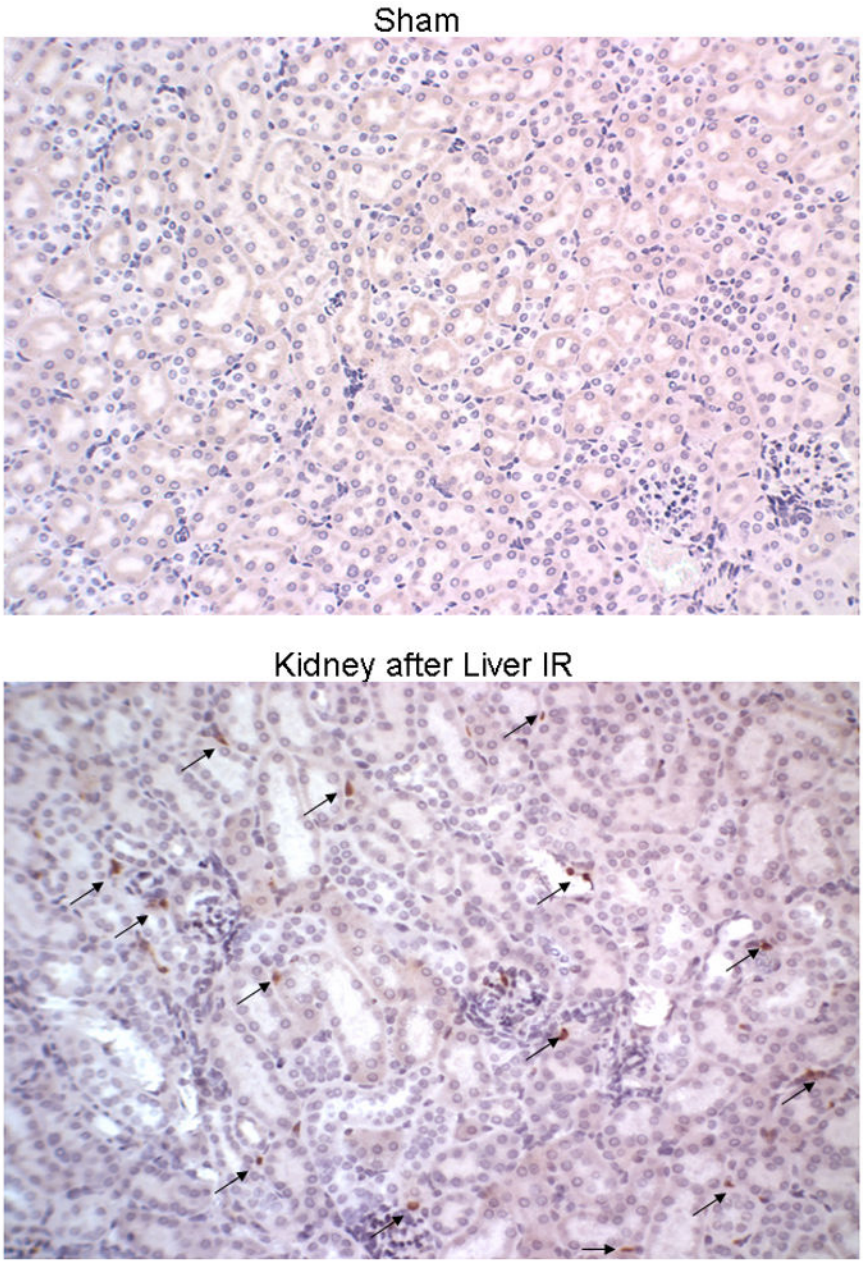

Figure 6.

Representative photomicrographs (100X) of 4 experiments of immunohistochemistry for neutrophil infiltration (arrows) in the outer medulla/inner cortex of the kidneys of C57BL/6 mice subjected to sham-operation or to 60 min. liver ischemia and 24 hr reperfusion.

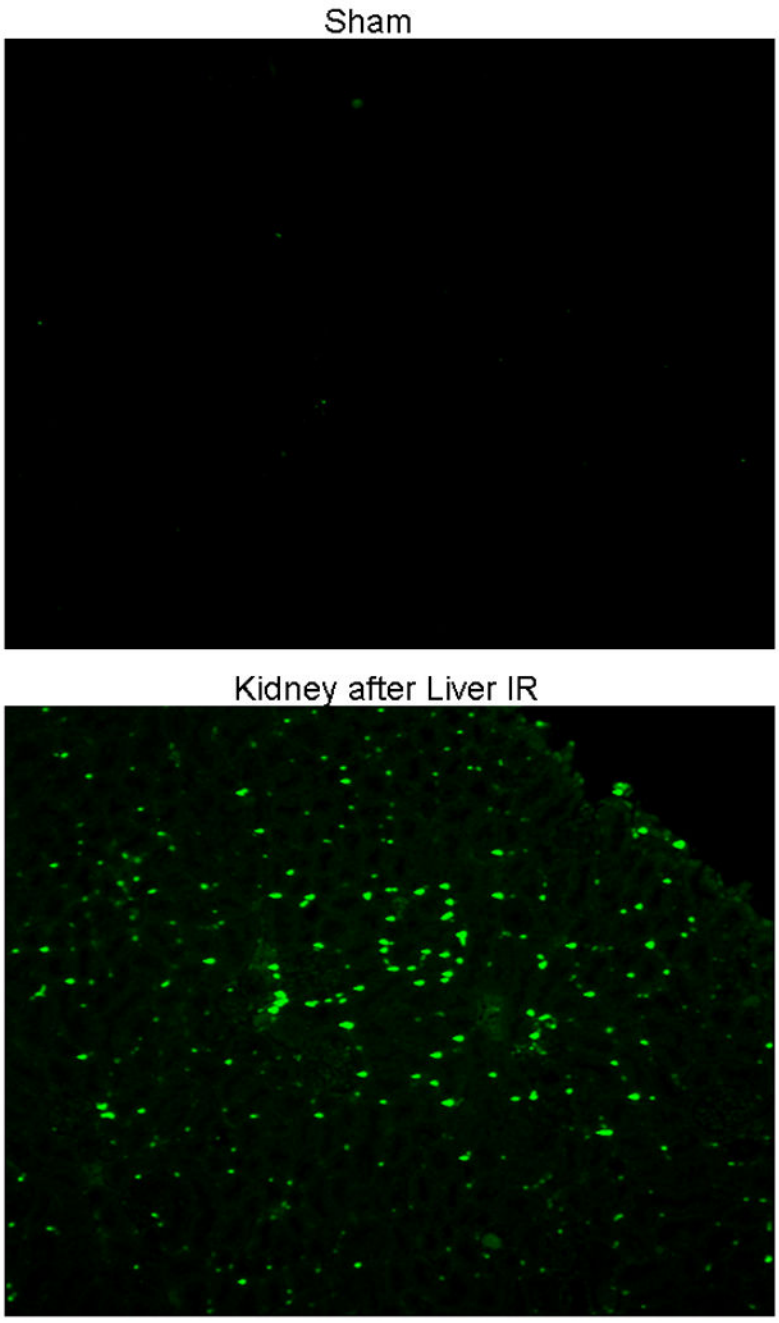

Figure 7.

Representative fluorescence photomicrographs (of 4 experiments) of kidney sections illustrating apoptotic nuclei [terminal deoxynucleotidyl transferase biotin-dUTP nick end-labeling (TUNEL) fluorescence staining, 100X]. C57BL/6 mice were subjected to sham-operation or to 60 min. liver ischemia and 24 hr reperfusion.

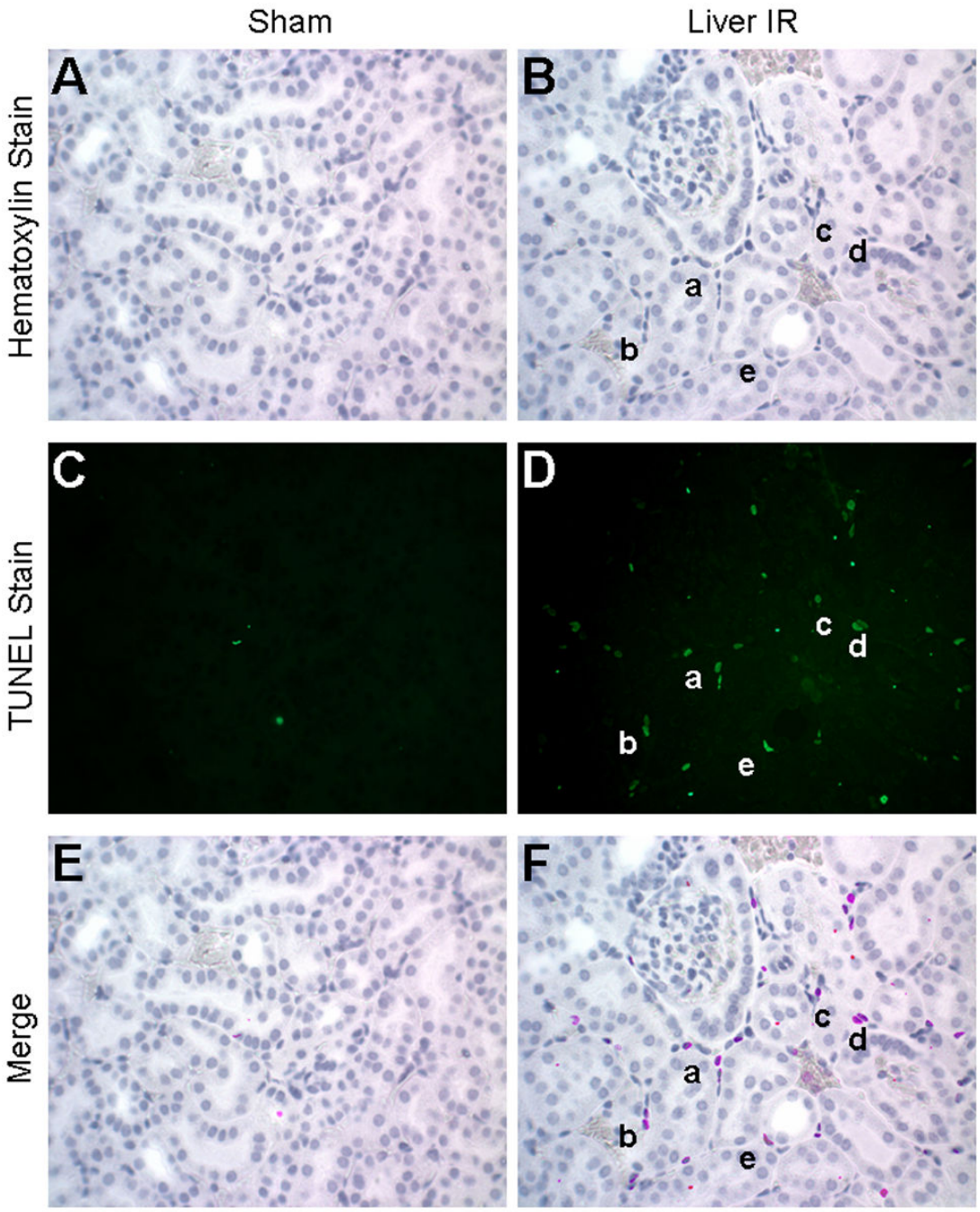

Figure 8.

Renal endothelial cell apoptosis after liver IR. C57BL/6 mice were subjected to sham-operation or to 60 min liver ischemia and 24 hr reperfusion. Top panel: Hematoxylin stain (400X) of kidneys from sham-operated mouse (A) or mouse subjected to liver IR (B). Middle panel: fluorescence photomicrographs of TUNEL staining from kidneys of mice subjected to sham-operation (C) or to liver IR (D). Bottom panel: Merge of A and C (Sham, E) revealed no evidence of apoptotic endothelial cells. In contrast, images from B and D (Liver IR) were merged (F) demonstrating apoptotic nuclei (represent in pink) within the

renal endothelial cells in the kidney of the mouse subjected to liver IR. Some of the endothelial cells are labeled **(a–e)** showing overlapping nuclear stain and apoptotic stain. Representative of 6 experiments.

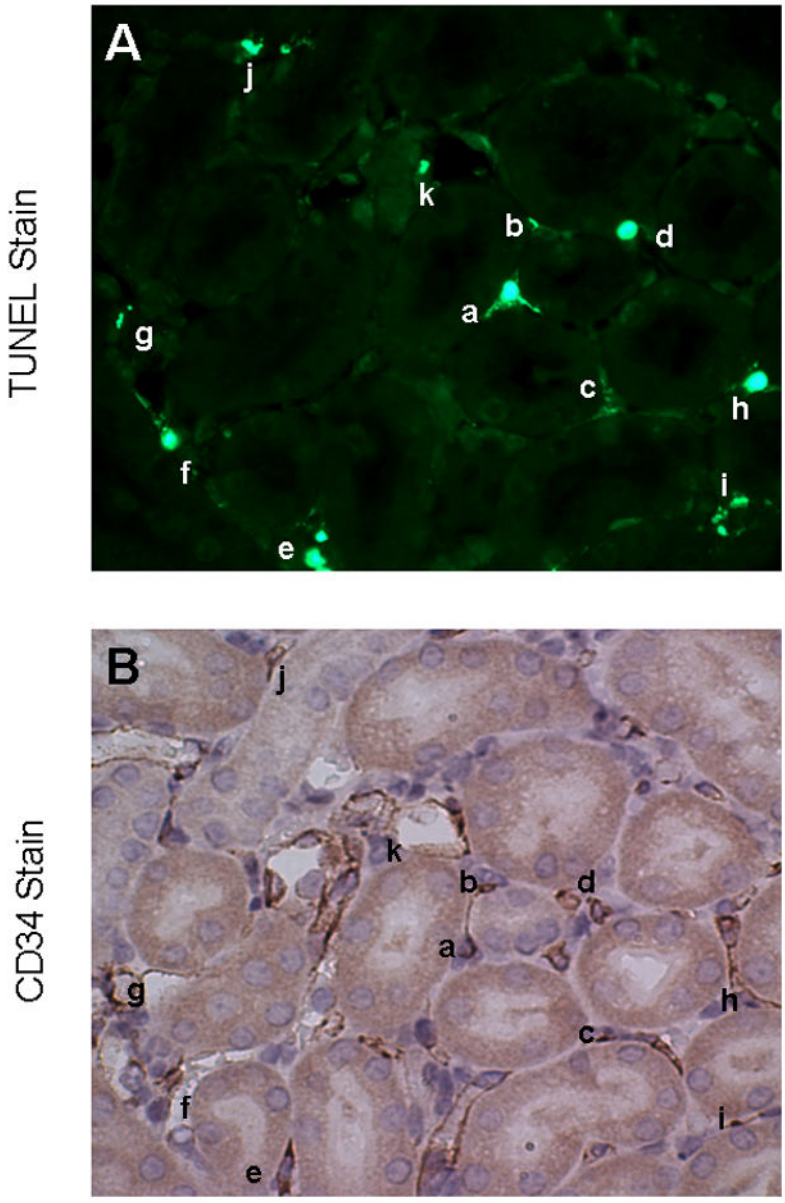

Figure 9.

Further confirmation of renal endothelial cell apoptosis after liver IR. C57BL/6 mice were subjected to 60 min liver ischemia and 24 hr reperfusion and serial kidney sections were stained with TUNEL (A) or with CD34 (an endothelial cell marker, B). TUNEL positive endothelial cells are labeled **(a–k)**. Representative of 4 serial sections stained.

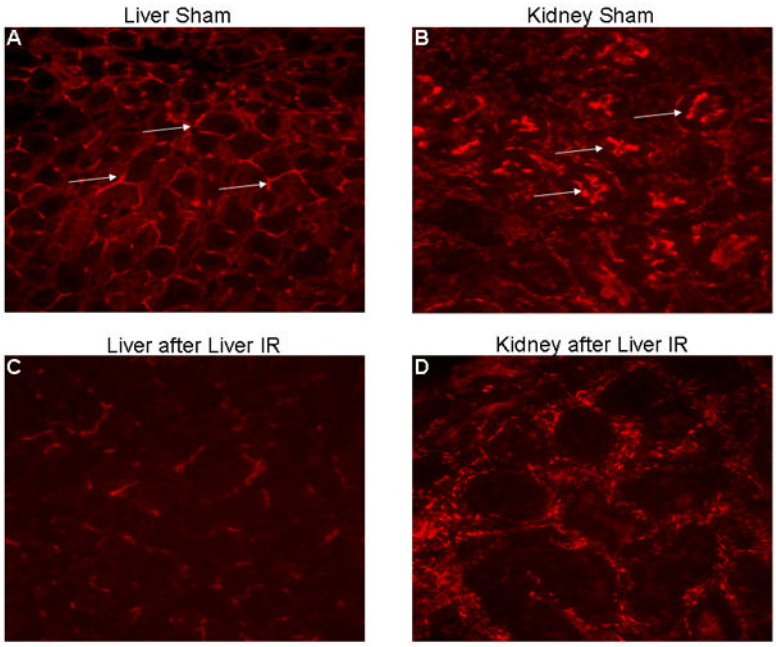

Figure 10.

Representative fluorescent photomicrographs of phalloidin labeling to visualize F-actin in the liver (A and C) and in the renal proximal tubules (B and D) from C57BL/6 mice subjected to sham-operation (A and B) or to 60 min. liver ischemia and 24 hr reperfusion (C and D). Representative of 6 independent experiments. Arrows represent some of the intact F-actin structure in the liver or in the renal proximal tubular epithelial cells.

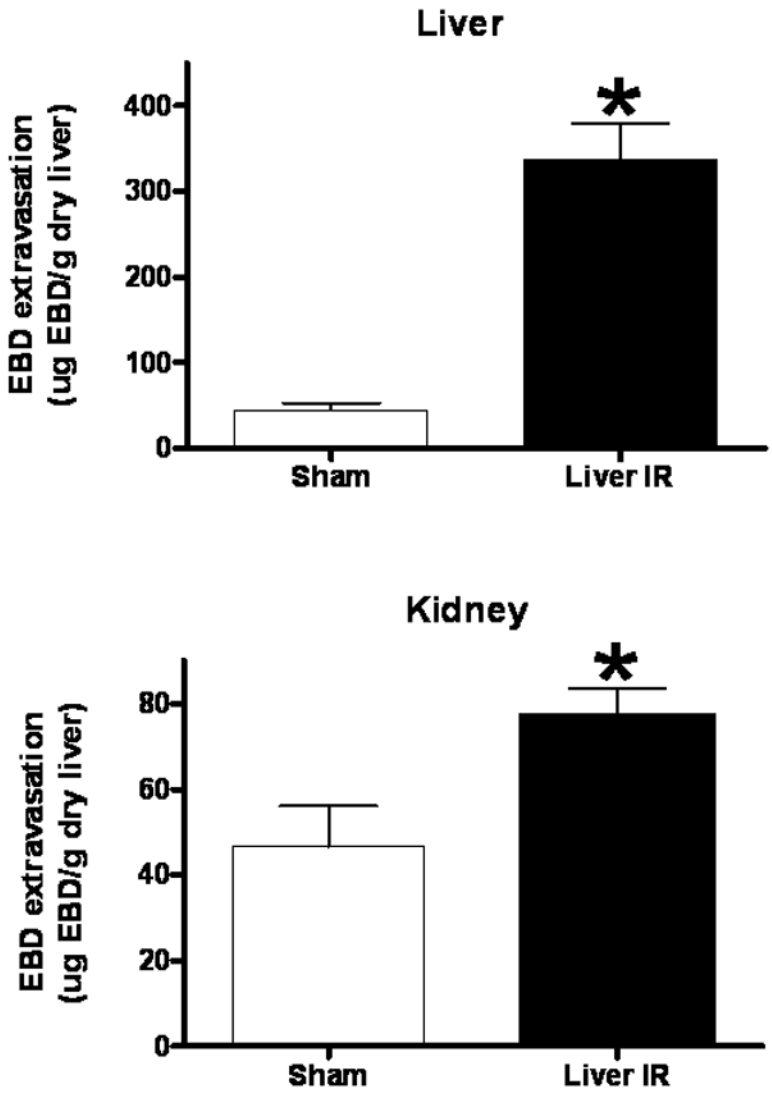

Figure 11.

Liver IR increases vascular permeability in the liver as well as in the kidney. C57BL/6 mice were subjected to sham-operation (N=6) or to 60 min. liver ischemia and 24 hr reperfusion (N=10). EBD was extracted in formamide and the amount of extravasated EBD concentration in kidney was calculated against a standard curve. * $p<0.05$ vs. sham-operated mice. Error bars represent 1 SEM.

Table 1

Primers used to amplify mRNAs encoding mouse GAPDH and pro-inflammatory cytokines based on published GenBank sequences for mice. Respective anticipated RT-PCR product size, PCR cycle number for linear amplification and annealing temperatures used for each primer are also provided. Abbreviations: KC = keratinocyte derived chemokine, MIP-2 = macrophage inflammatory protein 2, ICAM-1 = intercellular adhesion molecule-1, MCP-1 = monocyte chemoattractant protein 1, TNFα = tumor necrosis factor alpha.

Primer	Accession Number	Sequence (Sense, Antisense)	Product Size, bp	Cycle Number	Annealing T°C
Mouse KC	J04596	5′-CAATGAGCTGCGCTGTCAGTG -3′ 5′-CTTGGGGACACCTTTTAGCATC -3′	203	23	60
Mouse MIP-2	X53798	5′-CCAAGGGTTGACTTCAAGAAC -3′ 5′-AGCGAGGCACATCAGGTACG -3′	282	22	60
Mouse ICAM-1	X52264	5′-TGTTTCCTGCCTCTGAAGC -3′ 5′-CTTCGTTTGTGATCCTCCG -3′	409	21	60
Mouse TNF-α	X02611	5′-CCTCAGCCTCTTCTCCTTCCT -3′ 5′-GGTGTGGGTGAGGAGCA -3′	290	24	65
Mouse MCP-1	NM_011333	5′-ACCACAGTCCATGCCATCAC -3′ 5′-CACCACCCTGTTGCTGTAGCC -3′	312	22	60
Mouse GAPDH	M32599	5′-ACCACAGTCCATGCCATCAC -3′ 5′-CACCACCCTGTTGCTGTAGCC -3′	450	15	65